In *Rhodobacter sphaeroides* Reaction Centers, Mutation of Proline L209 to Aromatic Residues in the Vicinity of a Water Channel Alters the Dynamic Coupling between Electron and Proton Transfer Processes†

Julia Tandori,‡,§ Pierre Sebban,‡ Hartmut Michel,|| and Laura Baciou*,‡

Centre de Génétique Moléculaire, CNRS, Gif/Yvette, France, and Max-Planck-Institut für Biophysik, Frankfurt/Main, Germany

Received January 26, 1999; Revised Manuscript Received June 24, 1999

ABSTRACT: The X-ray crystallographic structure of the photosynthetic reaction center from *Rhodobacter sphaeroides* obtained at high resolution has revealed a number of internal water molecules (Ermler, U., Fritzsch, G., Buchanan, S. K., and Michel, H. (1994) *Structure 2*, 925−936; Stowell, M. H. B., McPhillips, T. M., Rees, D. C., Soltis, S. M., Abresch, E., and Feher, G. (1997) *Science 276*, 812−816). Some of them are organized into distinct hydrogen-bonded water chains that connect Q_B (the terminal quinone electron acceptor of the reaction center) to the aqueous phase. To investigate the role of the water chains in the proton conduction process, proline L209, located immediately adjacent to a water chain, was mutated to the following residues: F, Y, W, E, and T. We have first analyzed the effects of the mutations on the kinetic and thermodynamic properties of the rate constants of the second electron transfer ($k_{AB}(2)$) and of the coupled proton uptake (k_{H^+}) at the second flash. In all aromatic mutants, $k_{AB}(2)$ and k_{H^+} are notably and concomitantly decreased compared to the wild-type, while no effect is observed in the other mutants. The temperature dependence of these rates shows activation energy values ($\Delta H^{\ddagger}$) similar for the proton and electron-transfer processes in the wild-type and in most of the mutants, except for the L209PW and L209PF mutants. The analysis of the enthalpy factors related to the electron and proton-transfer processes in the L209PF and the L209PW mutants allows to distinguish the respective effects of the mutations for both transfer reactions. It is noteworthy that in the aromatic mutants a substantial increase of the free energies of activation is observed ($\Delta G^{\ddagger}_{L209PY} < \Delta G^{\ddagger}_{L209PF} < \Delta G^{\ddagger}_{L209PW}$) for both proton and electron-transfer reactions, while in the other mutants, $\Delta G^{\ddagger}$ is not affected. The salt concentration dependence of $k_{AB}(2)$ shows, in the L209PF and L209PW mutants, a higher screening of the protein surface potential experienced by Q_B. Our data suggest that residues F and W in position L209 increase the polarizability of the internal water molecules and polar residues by altering the organization of the hydrogen-bond network. We have also analyzed the rates of the first electron-transfer reaction ($k_{AB}(1)$), in the 100 μs time domain. These kinetics have previously been shown to reflect protein relaxation events possibly including proton uptake events (Tiede, D. M., Vazquez, J., Cordova, J., and Marone, P. M. (1996) *Biochemistry 35*, 10763−10775). Interestingly, in the L209PF and L209PW mutants, $k_{AB}(1)$ is notably decreased in comparison to the wild type and the other mutants, in a similar way as $k_{AB}(2)$ and k_{H^+}. Our data imply that the dynamic organization of this web is tightly coupled to the electron transfer process that is kinetically limited by protonation events and/or conformational rearrangements within the protein.

The photosynthetic reaction centers (RC) of purple bacteria are membrane- spanning energy-transducing proteins that convert solar energy into electrochemical energy by performing a transmembrane charge separation. The reaction center from *Rhodobacter (Rb.) sphaeroides* consists of three polypeptides L, M, and H. The L and M subunits bind noncovalently to the nine cofactors in 2-fold symmetric branches: four bacteriochlorophylls, two bacteriopheophytins, two ubiquinone molecules (Q_A and Q_B), and a non-heme iron Fe^{2+}. Two of the bacteriochlorophylls situated on the periplasmic side of the membrane are organized as a dimer (P) that acts as the primary photoinduced electron donor. The transmembrane charge separation is established between P (which is rapidly reduced by a soluble cytochrome c_2) and the primary electron acceptor quinone Q_A. The electron is transferred in a biphasic process from Q_A to the secondary electron acceptor quinone, Q_B (*1*, *2*). It has been proposed that the fast component (few μs) is due to "pure" electron-transfer reaction between the quinones, whereas the longer component (∼100−250 μs) reflects electron-transfer limited by protonation and/or conformational changes in the protein (*1*−*3*). The semiquinone state Q_B^- is stabilized by proton binding of surrounding residues that undergo a p*K* shift

† This work was supported by the Centre National de la Recherche Scientifique and by the Max-Planck Gesellschaft. J. T. was supported by the French Ministère des Affaires Etrangères.

* Corresponding author: Centre de Génétique Moléculaire, Bat. 24, CNRS, Gif/Yvette, France. Telephone/Fax: 33 1 69 82 38 26/38 02. E-mail: baciou@cgm.cnrs-gif.fr.

‡ Centre de Génétique Moléculaire.-

§ Present address: Department of Biophysics, József Attila University, Szeged, Hungary.

|| Max-Planck-Institut für Biophysik.

10.1021/bi990192e CCC: $18.00
Published on Web 09/14/1999

induced by the formation of the semiquinone state (*4*−*6*). The next photoinduced electron transfer leads to the formation of a doubly reduced quinone. The second electron-transfer reaction that is coupled to the uptake of two protons from the cytoplasm to Q_B, results in the protonation of the Q_B headgroup itself (*7, 8*). This process may involve the transient protonation state Q_BH (*9*). The dihydroquinone (Q_BH_2) is rapidly replaced by an oxidized quinone from the quinone pool present in the membrane (for reviews, see refs *10*−*13*).

The quinone Q_B is buried within the protein (∼15 Å from the protein surface) with no direct contact with the bulk phase. The translocation of the protons from the cytoplasm over long distances through the protein must involve chains of hydrogen-bonded donors and acceptors, the so-called proton wires (*14*). The high-resolution structures of the RC from *Rb. sphaeroides* and *Rhodopseudomonas viridis* have provided some evidence for such proton wires that may involve amino acid residues and/or hydrogen-bonded water molecules. Studying RC mutants has identified a few ionizable residues directly implicated in the proton transfer to Q_B. Studies achieved in RCs from *Rb. sphaeroides* where AspL213 and SerL223 were mutated to nonprotonatable residues have shown that these residues are involved in the transfer of the first proton to Q_B (*7, 8, 15, 16*). Similarly, studies of the GluL212→Gln mutant (*16*−*19*) have established that GluL212 is implicated in the second proton transfer to Q_B. Although the importance of these residues in the proton transfer to Q_B is clearly established, it has also been shown that in *Rb. capsulatus* and, more recently in *Rb. sphaeroides*, the protein can recover from the important handicap of the absence of these residues by additional electrostatic mutations (*19*−*21*), some of them are situated at more than 15 Å from Q_B close to the water chains. However, the lack of a continuous string of hydrogen-bonded protonatable residues long enough to connect Q_B to the bulk phase has led to consider the water molecules (*22*) as contributing to the web of the hydrogen-bond network. In the RC structure from *Rb. sphaeroides*, a chain of 14 ordered water molecules (initially described in ref *23*) may give access for protons to the interior of the protein (*23, 24*). These molecules are all at hydrogen bond distances and directly connect Q_B to the cytoplasm. More recently, the structure determination of the RC from *Rb. sphaeroides* at cryogenic temperature (*25*) has revealed another water chain connecting Q_B to the surface of the RC ending at the interface of the H and L subunits at the level of the lipid bilayer headgroups. While a contribution of ionizable and polar residues to proton transfer is likely (*26*), these arrangements of water chain molecules create an ideal hydrogen-bonded web from the Q_B site to the cytoplasmic surface. An extended three-dimensional hydrogen-bonded web has also been identified during the refinement of the *Rps. viridis* reaction center structure (*27*). The water molecules are excellent components of proton wires (*14, 28*). Computer simulations of proton translocations along a linear chain of water molecules have been carried out to understand the molecular mechanisms of proton conduction (*29, 30*). The protons were suggested to be transferred by a semi-delocalized process in which the protons are solvated over several (∼3−5) water molecules. In these studies, the importance of the connectivity and the cooperativity of the hydrogen-bond network was pointed out as an efficient proton transfer. Water wires appear to be involved in a number of proteins implicated in proton translocation. It has been proposed that water molecules could be involved in the proton-transfer pathway and in the protonation of the Schiff base of bacteriorhodopsin (*31, 32*). It has also been proposed that water molecules are important in the cytochrome b_6/f complex (*33*). In the cytochrome *c* oxidase, water molecules were also proposed to participate in the completeness of the proton wire (*34*−*36*). The questions of which intermediates are involved in the pathway, and how the proton motions through the protein are governed, are still open.

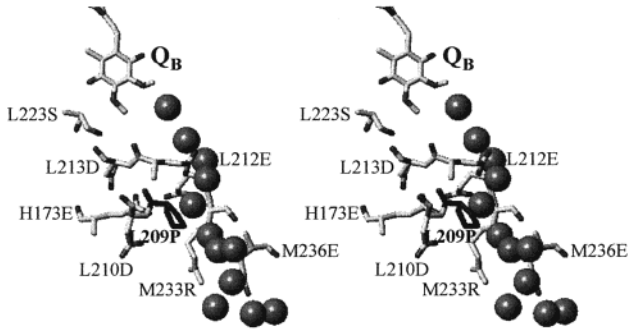

FIGURE 1: Stereoview of the arrangement of the water molecules (grey balls) in the vicinity of proline L209 (in black) in the reaction centers from *Rb. sphaeroides* (from ref *23*). Important residues mentioned in the text are indicated. The figure was produced with the program TurboFrodo (*59*).

To investigate the possible contribution of the water molecules in the proton conduction processes in the photosynthetic reaction center, techniques of mutagenesis (*37*) have been used in order to modify the continuity of the previously reported water chain. In the RC from *Rb. sphaeroides*, the amino acid residue proline L209 (Figure 1), located immediately adjacent to the water cluster w55 and w135 (*23*) was previously substituted by the aromatic residues PheL209PF and TyrL209PY (*37*). The substitution of the neutral residue proline L209 by an aromatic residue did not have drastic effects (such like photosynthetic incompetence) as observed when the terminal proton donors, such as AspL213 or GluL212, are absent. The major effect observed by the replacement of ProL209 with Tyr or Phe was a decreased rate of the second electron-transfer and the coupled proton transfer. The modification induced by the aromatic residue was suggested to be due to an alteration of the proton pathway, suggesting that in these mutants a nonspecific diffusion process for proton transfer may occur.

We present here the effect of the presence of different side chains at the position L209 (tyrosine, phenylalanine, tryptophane, glutamate, and threonine) on the functional properties of the RC. The L209PW mutant initially described in ref *38* is examined here in more detail. This work is focused principally in understanding the influence of the modified side chain at position L209 on the second electron-transfer reaction, on the coupled proton uptake process, and also on the first -flash electron-transfer process. The influence of the ionic strength on the electron kinetics was analyzed in the wild-type (WT) and in the mutant strains. The effect of temperature on the second electron and proton-transfer processes was also investigated. The results are discussed in terms of a disorganization of the hydrogen-bonded network due to the presence of aromatic residues at the position L209

resulting in decreased electron and proton-transfer capabilities.

MATERIALS AND METHODS

Bacterial Strains and Growth Conditions. All *Escherichia* (*E.*) *coli* strains were grown in LB medium supplemented with appropriate antibiotics. The *Rb. sphaeroides puf*Δ*L*MX21, originally the ATCC 17023 strain used in these studies, was previously described (*39*). *Rb. sphaeroides* wild-type or mutant strains harboring *puf*L mutation on pRK404 were grown in Erlenmeyer flasks filled to 50% of the total volume with malate yeast medium supplemented with kanamycin (20 μg/mL) and tetracycline (2 μg/mL). The cultures were grown in darkness at 30 °C on a gyratory shaker (*100 rpm*).

Genetic Methods. Site-directed mutagenesis was performed as described in ref *37*, using the method of Kunkel (*40*). For mutagenesis, pBSIIKS+ plasmid, which contains the puf operon, was used as a template. The mutagenic oligonucleotides were designed using *Rb. sphaeroides* codon preferences (*41*). After mutagenesis, the appropriate fragment carrying the desired mutation was cloned into the conjugation-proficient plasmid pRK404. This plasmid was introduced into *E. coli* strain S17-I (*42*) [*rec*A *pro*$^-$res$^-$mod$^+$Tp^r Sm^r pRP4-2-Tc::Mu-Km::*Tn*7]. Subsequently, the plasmid was transferred to the *Rb. sphaeroides puf*Δ*L*MX21 strain, and the transconjugants were selected for Kan^R and Tc^R (*43*). The same procedure was used for the construction of the deletion strain harboring the native *puf* operon. *E. coli* JM83 [F$^-$ *ara* Δ (*lac-pro*AB) *rps*L f80d*lac*ZΔ*M*15] and DH1 [F$^-$ *rec*A1 *end*A1 *gyr*A96 *thi*-1 *hsd*R17(r_K^-,m_K^+) *sup*E44 *rel*A1] were used as host strains for all standard cloning steps. Standard molecular biological methods were performed according to (*44*).

*Biochemical Techniques. Rb. sphaeroides puf*Δ*L*MX21 strains harboring native or mutations at L209 on the plasmid pRK404 were grown on a large scale as described above. The cells were harvested by centrifugation at 10 000 rpm for 10 min. The cell pellets were washed in 0.1 M sodium phosphate (pH 7.5) buffer, harvested, and stored at −80 °C. The cell pellet was resuspended in 20 mM Tris (pH 8) buffer and stirred 20 min in the presence of a spatula tip of DNAse and PMSF (1 mM). Then, the cells were disrupted by sonication, and the intracytoplasmic membranes (chromatophores) were purified as described in ref *37*. The pellets were resuspended in 20 mM Tris (pH 8) and diluted to a final concentration such that $A_{850} = 50$. A first membrane solubilization was done by addition of LDAO (Fluka Chemie) to a final concentration of 0.35% in the presence of 100 mM NaCl. The suspension was stirred 20 min at 26 °C in the dark. Nonsolubilized membranes were pelleted by centrifugation at 40 000 rpm and at 4 °C for 2 h. RCs were extracted by addition of LDAO on the resuspended pellet to a final concentration of 0.8% in similar conditions. The solubilized RCs were separated from the nonsolubilized materials by centrifugation for 2 h at 40 000 rpm and 4 °C. To increase the purity of the RCs, a precipitation with 22% NH_4 sulfate was done on the supernatant. The RCs containing a floating pellet was resuspended in 10 mM Tris (pH 8) buffer and was dialyzed overnight against 20 mM Tris-0.1% LDAO buffer. The RC extract was loaded onto a DEAE Sepharose CL-6B (Pharmacia) column prequilibrated with the same buffer. The column was washed in steps with the same buffer with increasing NaCl concentrations from step to step. The RCs were eluted at an ionic strength equivalent to 250 mM NaCl. The ratio of absorbance at 280/802 nm was in the range 1.5−1.8 for all RC preparations.

Electron and Proton-Transfer Measurements. $P^+Q_A^-$ and $P^+Q_B^-$ Charge Recombinations. Mutant RCs were characterized on a homemade spectrophotometer previously described (*45*). The decays of the $P^+Q_A^-$ and $P^+Q_B^-$ states were monitored at 865 nm following a Yag laser saturating flash at 532 nm. The $P^+Q_A^- \rightarrow PQ_A$ charge recombination rate (k_{AP}) was determined in the presence of terbutryn (200 μM). The $P^+Q_B^- \rightarrow PQ_B$ charge recombination rate (k_{BP}) was determined from the slow phase of recovery of the oxidized donor P^+ in RCs where the occupancy of the Q_B site was routinely restored by the addition of 60−100 μM UQ_6. The observed k_{AP} and k_{BP} values allow the determination of the one-electron-transfer equilibrium constant between $Q_A^-Q_B$ and $Q_AQ_B^-$ states, K_2, as given by eq 1 (*4*, *12*, *46*, *47*):

$$K_2 + 1 = k_{AP}/k_{BP} \quad (1)$$

The free energy barrier (ΔG°_{AB}) value between the $Q_A^-Q_B$ and the $Q_AQ_B^-$ states is given by eq 2:

$$\Delta G^\circ_{AB} = -k_B T \times \ln K_2 \quad (2)$$

where k_B is the Boltzman's constant and T is the absolute temperature.

First Electron-Transfer Measurements. The rate of the $Q_A^-Q_B \rightarrow Q_AQ_B^-$ first electron transfer ($k_{AB}(1)$) was measured at 753 nm by monitoring the absorbance changes in the bacteriopheophytin electrochromic band shift in the presence of excess UQ_6 (60−100 μM).

Second Electron-Transfer Measurements. The rate constant of the second electron-transfer $Q_A^-Q_B^- \rightarrow Q_AQ_B^{2-}$ ($k_{AB}(2)$) was determined by measuring the decay of the semiquinone absorption after the second flash at 450 nm in the presence of 40 μM horse heart cytochrome *c* and 1 mM sodium ascorbate. For complete reoxidation of Q_B, a 15 min dark adaptation time was applied to the samples between two successive measurements.

Proton Uptake Measurements. The proton uptake kinetics (k_{H^+}) after the second flash were measured (in the presence of 100 μM ferrocene as electron donor to P^+) in RCs dialyzed against 50 mM NaCl, 0.03% Triton X-100 during 36 h. Under these conditions, the Tris buffer concentration was kept below 10 μM. The proton binding kinetics by the RCs were measured by following the absorption changes at 582 nm (isosbestic point of P absorption) of the pH indicator dye, *o*-cresol red (40 μM). The final proton uptake signal was obtained with subtracting the buffered sample from the unbuffered signal.

Salt Titrations of $k_{AB}(2)$. Similar conditions were used as described above and the pH was adjusted at pH 7.5 ± 0.05. The pH of the bulk phase was controlled at each salt concentration. No significant variation of the pH was observed. The ionic strength was increased by adding successive aliquots of 3 M NaCl stock solution.

Temperature Dependencies of $k_{AB}(2)$ and k_{H^+}. The temperature of the sample was increased using a thermostat

Table 1: Kinetic and Energetic Characteristics of the Wild-Type and Mutated Reaction Centers from *Rb. sphaeroides* (pH 8.1 ± 0.05, 21 ± 0.5 °C)

strains	$k_{AP} \pm 0.3\ s^{-1}$[a]	$k_{BP} \pm 0.1\ s^{-1}$[a]	ΔG°_{AB}[b] ± 2 meV[a]	$k_{AB}(1)\ (s^{-1}) \pm 10\%$[a]	$k_{AB}(2)\ (s^{-1}) \pm 10\%$[a]	$k_{H^+}\ (s^{-1}) \pm 10\%$[a]
wild-type (L209P)	10.5	1.2	−52	7875	892	429
L209PT	10.3	1.7	−41	5350	775	675
L209PE	10.4	2.9	−24	5300	606	418
L209PY	10.1	1.5	−44	**6620**[c]	**325**[c]	**174**[c]
L209PF	10.8	1.1	−55	**917**	**79**	**106**
L209PW	10.9	7.5	+20	**75**	**34**	**42**

[a] Experimental errors [b] Calculated from eqs 1 and 2. [c] The kinetic parameters of the aromatic mutants are in bold.

apparatus and the pH of the sample (pH 8.1 ± 0.05) was checked at each temperature and readjusted if necessary.

Activation Parameters for the Electron ($k_{AB}(2)$) and Proton Transfer (k_{H^+}) Processes at the Second Flash. According to the Eyring model (*48*), the rate constant k_i (corresponding to $k_{AB}(2)$ or k_{H^+}) is correlated to the thermodynamic parameters of the electron or proton-transfer reactions by eq 3:

$$k_i = \frac{k_B T}{h} \times e^{-\Delta H^{\ddagger}/k_B T} \times e^{-\Delta S^{\ddagger}/k_B} \qquad (3)$$

where h is Planck's constant and $\Delta H^{\ddagger}$ and $\Delta S^{\ddagger}$ are the enthalpy and entropy changes associated to the reaction. The activation parameters are, therefore, determined by fitting the curves in a ($\ln(k_i/T)$ vs $(1/T)$) plot. $\Delta H^{\ddagger}$ and $T\Delta S^{\ddagger}$ are, respectively, derived by the slope and the intercept of the fitting line with the *y*-axis.

Depending on the pH range, the pH buffers used were MES (2-[*N*-morpholino] ethanesulfonic acid), Bistris-propane (1,3-bis[tris(hydroxymethyl)methylamino] propane), or CAPS (3-cyclohexylamino-1-propane sulfonic acid).

RESULTS

$P^+Q_A^-$ and $P^+Q_B^-$ Charge Recombination Kinetics and Free Energy Barrier between the $Q_A^-Q_B$ and the $Q_AQ_B^-$ States. In the presence of a competitive inhibitor to Q_B, the $P^+Q_A^-$ recombination rate constant was found to be essentially the same in the WT and the mutant RCs (k_{AP} = 10.1−10.9 s^{-1}; pH 8.1) (Table 1); k_{AP} is weakly pH dependent (data not shown). The k_{BP} values measured are shown in Table 1 at pH 8.1. The ΔG°_{AB} values deduced from the measurements of k_{AP} and k_{BP} for all strains are listed in Table 1. At pH 8.1, in most of the mutants, ΔG°_{AB} is nearly the same as in the WT. However, in the L209PE mutant, ΔG°_{AB} is decreased by 28 meV compared to the WT. In the L209PW mutant, since the $P^+Q_B^-$ recombination is fast, the slow phase is hardly resolved from the $P^+Q_A^-$ recombination. Therefore, a fixed value of k_{AP} (determined independently in the presence of terbutryn) was used for the fitting procedure of the $P^+Q_B^-$ recombination decay. In this mutant, an decrease of ΔG°_{AB} by about 70 meV was observed.

First and Second Electron-Transfer. The first electron-transfer rate constants ($k_{AB}(1)$) measured at 753 nm in all strains are shown in Table 1 (pH 8.1). A substantial decrease of the $k_{AB}(1)$ value is observed in the L209PF (10×) and in the L209PW (100×) mutants compared to WT. In the other mutants, this value is nearly not affected. The second electron-transfer rates were determined at 450 nm, after two laser flashes, from the decay of the semiquinone signal in the presence of exogenous electron donor (reduced cytochrome *c*) to P^+. The pH dependencies of $k_{AB}(2)$ for the mutants and for the native RCs are shown in Figure 2. The WT RCs behavior has been previously described (*37*). It displays a strong pH dependence for $k_{AB}(2)$, especially above pH 8. In the L209PT and L209PE mutants, the pH dependencies of $k_{AB}(2)$ are very similar to the WT. In the L209PW mutant (Figure 2), $k_{AB}(2)$ is substantially decreased (about 40×) compared to the WT. In the L209PY and L209PF mutants, $k_{AB}(2)$ was decreased 4× and about 15× at pH 8.1, respectively (*37*). Above pH 8, $k_{AB}(2)$ has a steeper slope in the L209PW mutant than in the WT. This behavior was also observed in the L209PY and L209PF mutants. In L209PW RCs, $k_{AB}(2)$ is proportional to $[H^+]^{0.9}$, whereas in native RCs, above pH 8, $k_{AB}(2)$ is proportional to $[H^+]^{0.6}$.

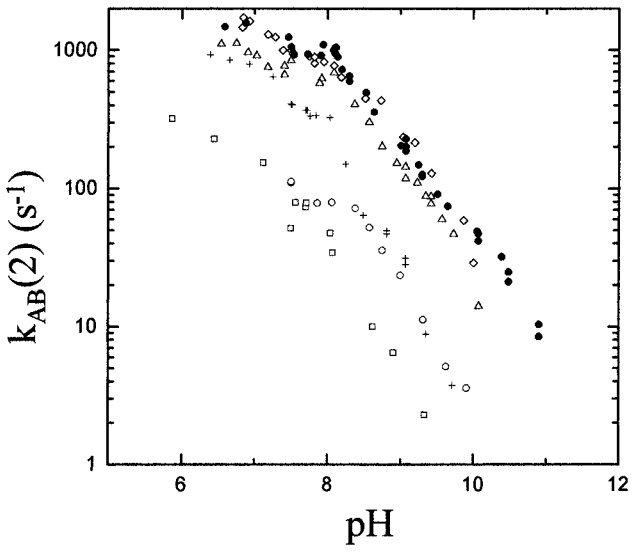

FIGURE 2: pH dependence of the second electron-transfer in the WT and mutant RCs (~2 μM) measured at 450 nm after a second flash: WT (●), L209PE (△), L209PT (◇), L209PY (+), L209PF (○) and L209PW (□). Conditions: 50 mM NaCl, 20 mM Tris, 0.1% LDAO, 40 μM cytochrome *c* and 1 mM sodium ascorbate. The pH buffers used were MES, bisTris-propane, or CAPS, depending on the pH range.

Salt Concentration Dependence of $k_{AB}(2)$. The effect of increasing salt concentration on $k_{AB}(2)$ is shown in Figure 3 for the mutants and for native RCs. The kinetics was measured from 0 to 600 mM NaCl at pH 7.5. In the WT, the rate was constant below 100 mM NaCl but decreased above this value. Over the studied salt concentration range, $k_{AB}(2)$ for the L209PE and L209PT mutants was very similar to the value measured in the WT. In the L209PY mutant, $k_{AB}(2)$ starts to decrease at lower salt concentration (40 mM NaCl). At variance, the L209PF mutant shows only a slight

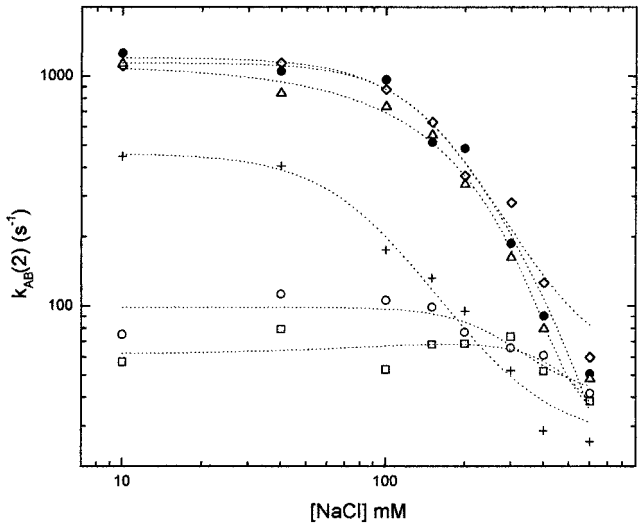

FIGURE 3: NaCl concentration dependence of the second electron-transfer rate in the WT and mutant RCs: WT (●), L209PE (△), L209PT (◇), L209PY (+), L209PF (○) and L209PW (□). Similar conditions used as in Figure 2, pH 7.5, 21 °C.

decrease of $k_{AB}(2)$ above 150 mM NaCl. Interestingly, nearly no variation of $k_{AB}(2)$ is observed in the L209PW mutant up to 600 mM NaCl.

Temperature Dependence of $k_{AB}(2)$ and of the Second Flash Proton Uptake (k_{H^+}). The temperature dependencies of the second electron-transfer kinetics and of the proton-transfer kinetics (k_{H^+}), measured at the second flash for each strain, are displayed in Figure 4. These data were acquired at pH 8.1, in the temperature range 275−310 K. The activation parameters derived from data shown in Figure 4 are presented in Table 2. In the WT and in the L209PT and L209PY mutants, the calculated enthalpy values for the electron-transfer process ($\Delta H^{\ddagger}(k_{AB}(2))$ are slightly higher by about 0.06 eV than the respective $\Delta H^{\ddagger}$ values for the proton-transfer process ($\Delta H^{\ddagger}(k_{H^+})$). The difference between $\Delta H^{\ddagger}$-($k_{AB}(2)$) and $\Delta H^{\ddagger}(k_{H^+})$ is significantly increased in the L209PE mutant (∼0.160 eV). At variance, in the L209PF and the L209PW mutants, the $\Delta H^{\ddagger}(k_{AB}(2))$ values are notably smaller than the corresponding $\Delta H^{\ddagger}(k_{H^+})$ values. This different behavior arises from the very low $\Delta H^{\ddagger}(k_{AB}(2))$ value in the L209PF mutant (0.139 ± 0.015 eV) and from the notably high $\Delta H^{\ddagger}(k_{H^+})$ value calculated in the L209PW mutant (0.520 ± 0.015 eV). It can be noted that the activation energy values derived from the Eyring and Arrhenius (data not shown) plots systematically differ by k_BT, as expected.

Although the enthalpic and entropic factors show notable variations among all the strains, the resulting free energies of activation ($\Delta G^{\ddagger}$) display quite firm values with much less variations. The much smaller error bars on the free energies, reflect the "compensating" effects. Similar large changes in $\Delta H^{\ddagger}$ that are not reflected in changes in $\Delta G^{\ddagger}$ due to enthalpy−entropy compensation were previously highlighted for the charge recombination processes in the photosynthetic

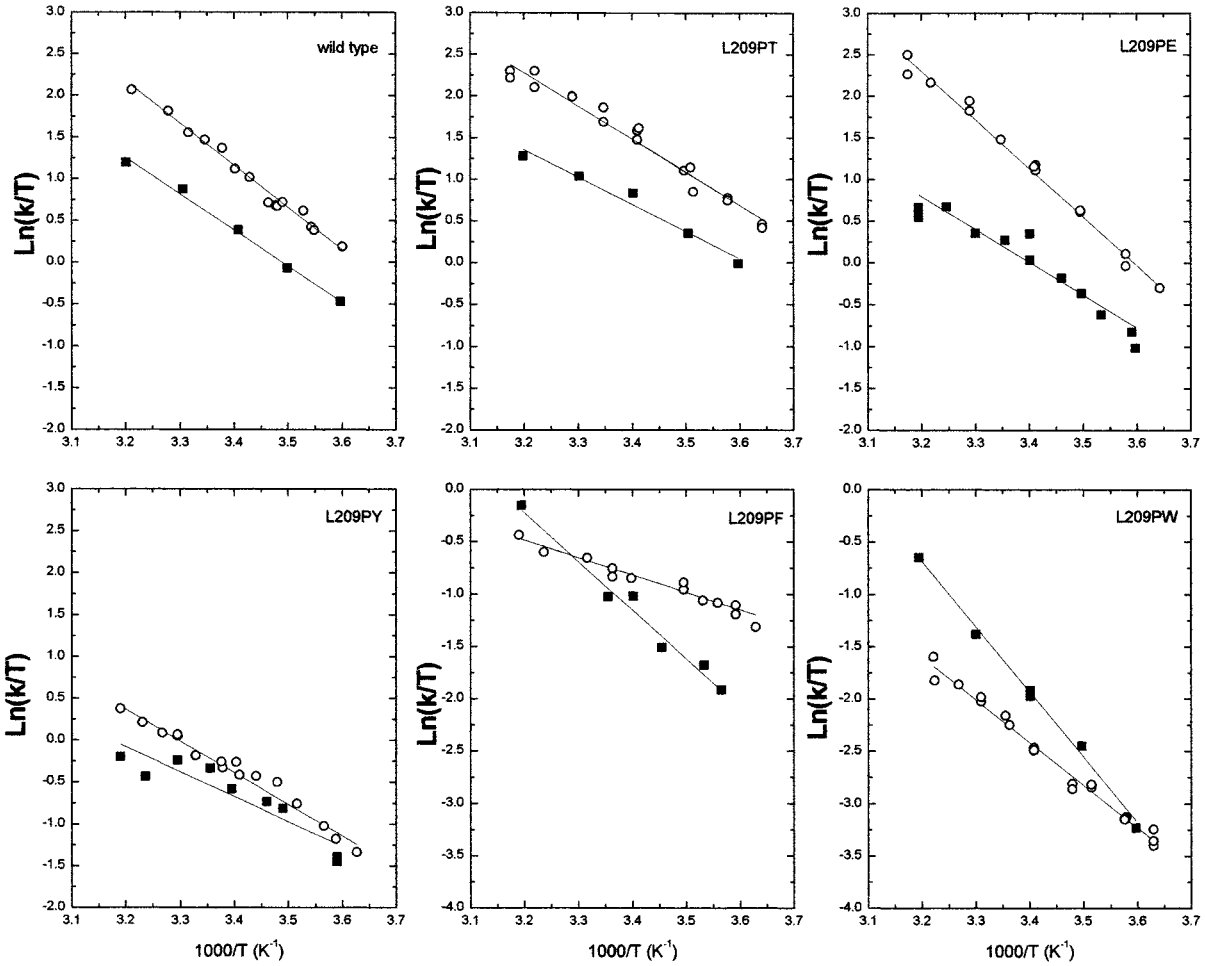

FIGURE 4: Comparison of the Eyring plots of second electron-transfer (open symbols; 450 nm) and second flash proton uptake (closed symbols; 582 nm) kinetics in the WT and mutant RCs measured at pH 8.1 ± 0.05. Conditions: see in Materials and Methods.

Table 2: Thermodynamic Parameters Associated to the Second Electron-Transfer and to the Proton Uptake Measured at the Second Flash in the WT and the Mutant RCs (pH 8.1 ± 0.05)[a]

strains	$\Delta H^{\ddagger}(k_{AB}(2)) \pm$ 0.010 eV[b]	$T\Delta S^{\ddagger}(k_{AB}(2)) \pm$ 0.010 eV[b]	$\Delta G^{\ddagger}(k_{AB}(2)) \pm$ 0.002 eV[b]	$\Delta H^{\ddagger}(k_{H^+}) \pm$ 0.010 eV[b]	$T\Delta S^{\ddagger}(k_{H^+}) \pm$ 0.010 eV[b]	$\Delta G^{\ddagger}(k_{H^+}) \pm$ 0.002 eV[b]	$\delta\Delta H^{\ddagger}(k_{AB}(2) - k_{H^+}) \pm$ 0.020 eV[b]
wild-type	0.420	−0.135	0.555	0.360	−0.216	0.576	0.060
L209PT	0.331	−0.218	0.549	0.272	−0.298	0.570	0.059
L209PE	0.486	−0.069	0.555	0.327	−0.259	0.587	0.159
L209PY	**0.315**[c]	**−0.282**[c]	**0.596**[c]	**0.248**[c]	**−0.357**[c]	**0.605**[c]	**0.067**[c]
L209PF	**0.139**	**−0.472**	**0.611**	**0.387**	**−0.227**	**0.614**	**−0.248**
L209PW	**0.340**	**−0.307**	**0.647**	**0.520**	**−0.112**	**0.632**	**−0.180**

[a] Values determined from Eyring plots fitted with eq 3. [b] Experimental errors. [c] The parameters related to the aromatic mutants are presented in bold.

RCs from *Rps. viridis* (*49*−*51*). The $\Delta G^{\ddagger}(k_{AB}(2))$ values derived for the WT, the L209PT, and the L209PE RCs are identical (0.555 eV) within the error bars. Interestingly, compared to the WT, in the L209PY, L209PF, and L209PW mutants, the $\Delta G^{\ddagger}(k_{AB}(2))$ values are increasing as (Table 2): L209PY (0.596 eV) < L209PF (0.611 eV) < L209PW (0.647 eV). The same overall trend is observed for the $\Delta G^{\ddagger}(k_{H^+})$ values. The $\Delta G^{\ddagger}(k_{H^+})$ values are nearly the same for the WT (0.576 eV), the L209PT (0.570 eV), and L209PE (0.587 eV) mutants. At variance, a notable increase of these values is measured in the aromatic mutants, with the $\Delta G^{\ddagger}(k_{H^+})$ values increasing as: L209PY (0.605 eV) < L209PF (0.614 eV) < L209PW (0.632 eV).

DISCUSSION

Proline at position 209 of the L subunit of RC from *Rb. sphaeroides* is situated at the beginning of the "de" non-membrane-spanning helix. This proline is not conserved in the homologue protein from *Rps. viridis* (where the corresponding analogue residue is an alanine). It is, therefore, likely that ProL209 is not crucial for the structural organization of the RC. ProL209 is located in the proximity to a large network of water molecules (in hydrogen bond distances; see Figure 1), which was revealed by X-ray crystallographic studies (*23, 25*). Water w55 and w135 (the water molecules are numbered as in ref *23*) are the closest neighbors to PL209.

Our previous studies achieved on L209PY and L209PF (*37*) showed a significant effect on the rate constant of the proton-coupled second electron-transfer to Q_B. We have suggested that in these mutants, the aromatic residues introduced at position L209 have induced a perturbation of the proton pathway. To further examine this hypothesis, we have investigated the effects of substitution of ProL209 by different amino acids (T, E, Y, F, and W) on the kinetics and energetics of the first and second electron-transfer and of the coupled proton uptake at the second flash.

Energetic Effects of the Mutations. As shown in Table 1 at pH 8.1, the equilibrium constant values between the $Q_A^-Q_B$ and $Q_AQ_B^-$ states are similar to the WT in most of the mutant RCs, except for the L209PE and L209PW mutants. Both mutants exhibit a smaller magnitude for ΔG°_{AB} value than in the WT. The decreased magnitude for ΔG°_{AB} by about 28 meV in the L209PE mutant (Table 1) may reflect a slightly more negative potential experienced by Q_B^- compared to the wild-type. Such a small change may arise from a partial negative charge carried by the glutamate side chain at pH 8.1. Alternatively, the destabilization may be related to the presence of protonatable residues nearby the position L209 (within 3−5 Å) like GluL212, AspL213, AspL210. These residues have been suggested by the calculations (*52, 53*) to form a highly interacting cluster. The introduction of a glutamate side chain may have induced a slight change of the charge distribution within the cluster bringing its negative charge closer to Q_B.

In contrast to the other aromatic mutants (L209PY and L209PF), in the L209PW mutant, the magnitude for ΔG°_{AB} is strongly reduced to +20 meV. In this mutant, the estimation of ΔG°_{AB} is less meaningful since the k_{BP} value is close to the k_{AP} value. It is likely that the nature and the structure of the environment of the potentially titratable residues or water molecules are modified in the mutated protein compared to the WT. Indeed, the Pro→Trp mutation may reveal the presence of some (negative) ionizable residues that are poised (or neutralized) by electrostatic interactions in the WT. It is also possible that some structural reorganizations of the above-mentioned cluster have occurred. This charge rearrangement would result into an increase of the negative charge density in the Q_B vicinity, thereby destabilizing Q_B^-. A similar explanation was suggested to account for the effect of the GluH173→Gln mutation from *Rb. sphaeroides* (*54*).

Proton Motion-Coupled to the Second Electron-Transfer. The L209PE and L209PT mutations do not affect the $k_{AB}(2)$ values, which run closely to the pH dependence of the WT. The putative negative charge carried by GluL209 does not apparently alter the hydrogen-bond network involved in the proton delivery to Q_B.

In contrast, in all aromatic mutants, $k_{AB}(2)$ is notably decreased compared to WT as following: $k_{AB}(2)$(L209PY) > $k_{AB}(2)$(L209PF) > $k_{AB}(2)$(L209PW) (see Table 1 and Figure 2). In these mutants, the proton uptake rate constants measured at the second flash are decreased to the same extent as the $k_{AB}(2)$ values (see Table 1). It is well-established that the second electron-transfer is kinetically coupled to the first proton-transfer to Q_B. The results obtained here in the L209PF and L209PW mutants, suggest that the mutations alter at least the pathway of the first proton-transfer. It might be that the introduction of an aromatic residue disturbs the local structure of the hydrogen-bond network, involving protonatable residues and/or water molecules making the configuration of the environment less active for proton transfer and delivery. This might also be explained by an altered energetics for proton transfer due to an unfavorable (but fast) uphill proton-transfer step whose energy level has been increased.

It should be noted that, at pH 8.1 as shown in Figure 4, in the WT, the L209PT, and L209PE mutants, the k_{H^+} values

are significantly smaller (about 2−3×) than the respective $k_{AB}(2)$ values. This difference is observed over the entire temperature range. In the L209PY mutant, the difference between k_{H^+} and $k_{AB}(2)$ is smaller. More surprisingly, but directly correlated to different $\Delta H^{\ddagger}(k_{H^+})$ and $\Delta H^{\ddagger}(k_{AB}(2))$ values (discussed below; Table 2), in the L209PF mutant (above 28 °C) and in the L209PW mutant, k_{H^+} is found higher than the respective $k_{AB}(2)$ suggesting that the two processes are less coupled than expected from the WT measurements. This suggests that a nonnegligible amount of protons is taken up from the exterior by the RC before the second electron arrives on Q_B. This proton uptake event is coupled to the arrival of the electron on the primary electron acceptor, Q_A. In this case, internal proton-transfer may be sufficient to allow the second reduction of Q_B to occur. This feature is under current investigations.

Salt Effect on the Second Electron-Transfer Reaction. In the WT, the addition of NaCl has no effect on $k_{AB}(2)$ up to 100 mM at pH 7.5. Above this concentration, $k_{AB}(2)$ starts to decrease (Figure 3). A decrease of the $k_{AB}(2)$ value upon increased salt concentration may be correlated to an effect on the surface pH due to a screening of the negative groups of the protein surface. This decreases the surface proton concentration and thus increases the (local) pH seen by the RC (*55, 56*) (without bringing about a change in the solution pH). Thus, decreasing the surface potential by increasing the ionic strength helps revealing the presence of internal groups. These groups have their p*K*s shifted to lower pH and consequently modulate the $k_{AB}(2)$ value. These groups might be involved in the pH dependence of $k_{AB}(2)$ in Figure 2. In the WT, if we assume that the salt has an influence entirely through the surface potential on the apparent p*K* values of ionizable groups, the comparison of the salt concentration dependence of $k_{AB}(2)$ with its pH dependence, suggests a shift in surface pH of 0.5 pH units/100 mM NaCl. In the *Rb. sphaeroides* WT, using monovalent cations, a similar salt concentration dependence was observed for the second flash-induced quinone phase using electrogenic detection method (*56*). The same salt concentration dependence was obtained for the H^+ binding rate associated to the formation of the $P^+Q_A^-$ state (*55*). These authors have modeled high-salt effects on the kinetics of H^+ binding using a Gouy−Chapman approach, suggesting that the effect occurs via the mobile counterion distribution at the surface of the protein. It is reasonable to interpret the effect on $k_{AB}(2)$ seen here in a similar manner.

In the WT and in the L209PT and L209PE mutants, the salt concentration dependencies are identical. Thus, the apparent p*K* of the ionizable residues implicated in the variations of $k_{AB}(2)$ are modulated to the same extent in the WT, the L209PE and L209PT mutants by high concentration of cations at the protein surface. The situation is slightly different in the L209PY mutant. Here, the slope of $k_{AB}(2)$ vs [NaCl] is smaller than in the WT. This effect is reversed in the titration of $k_{AB}(2)$ vs pH where the slope in the L209PY mutant is steeper than in the WT. This suggests a smaller influence of the surface charge in the RC from the L209PY mutant than in the WT. In addition, it might be noted that in this mutant, $k_{AB}(2)$ starts to decrease at a lower salt concentration than in the WT. This may appear in contradiction with the similar apparent p*K*s observed in the pH dependence curves of $k_{AB}(2)$ in the WT and in the L209PY mutant. This apparent discrepancy may reveal the presence of an additional p*K* group in the L209PY mutant, which is more sensitive to the influence of external charges. This group (to which the hydroxyl group present in the tyrosine side chain may actively participate) may be situated closer to the exterior than the group that modulates $k_{AB}(2)$ in the pH dependence of the WT.

It is noteworthy that in the L209PF and L209PW mutants, $k_{AB}(2)$ is nearly salt independent in the studied salt concentration range. In both cases, a slight decrease of $k_{AB}(2)$ is observed at high-salt concentration but with smoother dependencies than in the WT and even than in the L209PY mutant. The observed effect on the L209PF and L209PW mutants reveals a higher screening of the salt effect inside the protein. The apparent increase of the dielectric constant in the cytoplasmic part of the protein may result from an increased polarizability of the proteic matrix. The introduction of aromatic residues may have partly disorganized the hydrogen-bond network to which structured water molecules participate. This allows a higher mobility of their dipolar moments and may, therefore, explain the important screening effect of the surface potential in the L209PF and L209PW mutants. In the L209PY mutant, the effect is attenuated. This may be due to the ability of the hydroxyl group to develop hydrogen bonds with its environment, therefore, reducing the disorganization effect observed in the two others aromatic mutants.

First Electron-Transfer Reaction. It has been pointed out, initially by Tiede et al. (*2*), that the kinetics of the $Q_A^-Q_B \rightarrow Q_AQ_B^-$ electron-transfer reaction are heterogeneous. This effect was measured in chromatophores from *Rb. sphaeroides* in the near-infrared in the bacteriopheophytin electrochromic band shift at 750 nm. In isolated RCs, a similar effect was detected when Q_A was replaced by low potential quinones (*1*). Interestingly, in these works, the fast component (few μs) was assigned to a "pure" electron-transfer reaction. At variance, longer components ($\geq 100\ \mu$s) were assigned to electron-transfer processes kinetically limited by protonation and/or conformational events within the protein. Additional support to this hypothesis has recently been provided (*3*). It is, therefore, of high interest that the ProL209→Phe and ProL209→Trp mutations display substantially reduced $k_{AB}(1)$ rates compared to the WT. This suggests that the perturbations induced by these mutations are structurally and dynamically coupled to the protonation and/or conformational process which kinetically limits the $Q_A^-Q_B \rightarrow Q_AQ_B^-$ electron-transfer reaction. Since these mutations are likely to affect not only the network of hydrogen bonds involving water molecules (*37*) but also ionizable and polar groups, we suggest that it exists a direct coupling between the dynamic structure of this web and the functional capabilities of the protein to rapidly transfer the electron from Q_A^- to Q_B. It is of importance to note that the crystal structure of the L209PF and L209PY mutants reveals no changes in the protein backbone (Kuglstatter, A., Fritzsch, G., Baciou, L., and Michel, H., unpublished data). This supports that the modifications of the coupling that we suggest here is not due to major structural protein rearrangements in the mutants but rather to a local disorganization of the hydrogen-bond network connectivity.

Furthermore, the decrease of the $k_{AB}(1)$ rates measured in the PL209F and PL209W mutants compared to the wild-

type is reminiscent to what we measure for the $k_{AB}(2)$ and k_{H^+} rates. This suggests that these mutations most likely affect the first and second electron-transfer reactions kinetically limited by protonation events. This is under further experimental investigations.

Temperature Dependence of the Electron-Transfer and the Associated Proton Uptake on the Second Flash. In the WT and in the L209PT and L209PY mutants, the $\Delta H^{\ddagger}$ values of $k_{AB}(2)$ and k_{H^+} are similar. This result supports the idea that electron- and proton-transfer reactions undergo the same rate limiting steps. This is not the case for the L209PE, L209PF, and L209PW mutants. The effects of the mutated side chain are selectively different on the electron and on the proton-transfer processes. The mutation L209PF causes a significant decrease of the $\Delta H^{\ddagger}(k_{AB}(2))$ value, whereas the $\Delta H^{\ddagger}(k_{H^+})$ value is essentially unchanged compared to the WT. Thus, the substitution of Pro by Phe specifically affects the electron-transfer reaction to Q_B. Conversely, in the L209PW mutant, the $\Delta H^{\ddagger}(k_{AB}(2))$ is only slightly decreased compared to WT while the $\Delta H^{\ddagger}(k_{H^+})$ value is significantly increased. This might be explained by an energetically unfavorable proton conduction pathway in the L209PW mutant. In the L209PE mutant, a difference between the $\Delta H^{\ddagger}(k_{AB}(2))$ and $\Delta H^{\ddagger}(k_{H^+})$ value is also observed (Table 2) but less marked than in the L209PW and L209PF mutants. In the L209PE mutant, it is likely that the negative charge that is probably carried by the glutamate side chain facilitates the proton transfer, while it impedes the electron flow. The enthalpy effect of the mutation (F, W, or E) on respectively the electron and on the proton-transfer processes suggest that both events can be separated thermodynamically.

Remarkably, despite the large changes of the $\Delta H^{\ddagger}$ and $\Delta S^{\ddagger}$ values, only very weak variations are observed in the $\Delta G^{\ddagger}$ values calculated for the proton or the electron processes (Table 2) in the WT, the L209PT, and L209PE mutants. It is, therefore, noteworthy that, when aromatic residues are introduced at the position L209, $\Delta G^{\ddagger}$ is increased in parallel (Table 2) for electron and proton-transfer reactions as following $\Delta G^{\ddagger}$(L209PY) < $\Delta G^{\ddagger}$(L209PF) < $\Delta G^{\ddagger}$(L209PW). The effect of the aromatic residues on the $\Delta G^{\ddagger}$ can be ascribed in part to changes in dynamics of the proton wire and of the degree of connectivity of the hydrogen-bond network implicated in the proton-transfer pathways. The fast proton-transfer kinetics observed in the wild-type compared to the mutants suggest that structured water and/or protonatable residues are arranged in an optimized configuration of their dipole−dipole and hydrogen-bonding interactions. The introduction of aromatic residues may have disorganized the interactions between the hydrogen bond donors and acceptors. This disorganization decreases the cooperativity for the proton-transfer mechanism. The importance of the cooperativity between donor and acceptor for proton-transfer reaction have been emphasized by molecular dynamic calculations (*57*). These authors have shown that the complete transport of a charge along a proton wire requires two complementary processes. The first is described as an ionic defect (translocation of an excess proton). The second involves a reorientation of the hydrogen-bonded chain (bonding defect). In contrast to the ion translocation, the authors suggest that a bonding defect, which is directly due to the surrounding protein, constitutes the kinetically limiting step for proton transfer along the wire. We suggest, here, that the main effect of the aromatic groups is to operate as a defect along the hydrogen-bond network.

CONCLUSION

The L209PF and L209PW mutants display kinetic, electrostatic, and thermodynamic properties significantly different from the WT and the other mutants analyzed in this work. The introduction of these aromatic residues in position L209 induce a parallel slowing down of the electron- and proton-transfer kinetics observed at the second flash and of the electron-transfer kinetics measured on the first flash. This suggests that these mutations most likely affect electron -transfer reactions that are kinetically limited by protonation events. We shall soon report data that support the presently suggested effect of the aromatic mutations on the proton conduction pathways. Recent numerical calculations (*58*) have suggested that the $Q_A^- Q_B \rightarrow Q_A Q_B^-$ electron-transfer process induces motions of structured water molecules situated nearby the channels revealed in the 3D structure of the protein, in particular the one that we are presently affecting by the L209 mutations. This is in strong support of our work, which suggests that the aromatic mutations at the L209 site affect the protonation events and/or conformational gating kinetically coupled to the electron-transfer reaction.

The salt titration and temperature dependence of $k_{AB}(2)$ and k_{H^+} suggest for the L209PF and L209PW mutants a disorganization of the hydrogen-bond network that connects Q_B to the cytoplasm and an increased degree of freedom of the participating groups. This suggests that an optimized organization of the proton donors and acceptors (which involve water molecules or protonatable residues) is essential to guarantee a fast proton transfer. Water molecules that are more mobile than side chains may ensure the good connectivity of the large hydrogen bond network structure and a high cooperativity for efficient proton conduction. These two requirements are disturbed in the aromatic mutants.

It will be of great interest to track the motions and rearrangements of structured water molecules and amino acid residues within the hydrogen-bond web in response to the different redox states of the RC protein. Such kinds of function−structure investigations should also be worth studying in other similar redox proteins.

ACKNOWLEDGMENT

We thank Drs. M. R. Gunner, E. Alexov, A. Gerschel, G. Fritzsch, and A. Kuglstatter for helpful discussions. A. K. is also thanked for careful reading of the manuscript.

REFERENCES

1. Li, J., Gilroy, D., Tiede, D. M., and Gunner, M. R. (1998) *Biochemistry 37*, 2818−29.
2. Tiede, D. M., Vazquez, J., Cordova, J., and Marone, P. A. (1996) *Biochemistry 35*, 10763−75.
3. Graige, M. S., Feher, G., and Okamura, M. Y. (1998) *Proc. Natl. Acad. Sci. U.S.A. 95*, 11679−84.
4. Wraight, C. A. (1979) *Biochim. Biophys. Acta. 548*, 309−327.
5. Maroti, P., and Wraight, C. A. (1988) *Biochim. Biophys. Acta. 934*, 329−347.
6. McPherson, P. H., Okamura, M. Y., and Feher, G. (1988) *Biochim. Biophys. Acta. 934*, 348−368.

7. Takahashi, E., and Wraight, C. A. (1990) *Biochim. Biophys. Acta. 1020*, 107−111.
8. Paddock, M. L., McPherson, P. H., Feher, G., and Okamura, M. Y. (1990) *Proc. Natl. Acad. Sci. U.S.A. 87*, 6803−7.
9. Graige, M. S., Paddock, M. L., Bruce, J. M., Feher, G., and Okamura, M. Y. (1996) *J. Am. Chem. Soc. 118*, 9005−9016.
10. Okamura, M. Y., and Feher, G. (1992) *Annu. Rev. Biochem. 61*, 861−96.
11. Okamura, M. Y., and Feher, G. (1995) in *Anoxygenic Photosynthetic Bacteria* (Blankenship, R. E., Madigan, M. T., and Bauer, C. E., Eds.) pp 557−594, Kluwer Academic Publishers.
12. Shinkarev, V. P., and Wraight, C. A. (1993) in *The Photosynthetic Reaction Center* (Norris, J. R., and Deisenhofer, J., Eds.) pp 193−255, Academic Press.
13. Sebban, P., Maróti, P., and Hanson, D. K. (1995) *Biochimie 77*, 677−94.
14. Nagle, J. F., and Morowitz, H. J. (1978) *Proc. Natl. Acad. Sci. U.S.A. 75*, 298−303.
15. Paddock, M. L., Rongey, S. H., McPherson, P. H., Juth, A., Feher, G., and Okamura, M. Y. (1994) *Biochemistry 33*, 734−45.
16. Rongey, S. H., Paddock, M. L., Feher, G., and Okamura, M. Y. (1993) *Proc. Natl. Acad. Sci. U.S.A. 90*, 1325−9.
17. Paddock, M. L., Rongey, S. H., Feher, G., and Okamura, M. Y. (1989) *Proc. Natl. Acad. Sci. U.S.A. 86*, 6602−6.
18. Takahashi, E., and Wraight, C. A. (1992) *Biochemistry 31*, 855−66.
19. Miksovska, J., Kálmán, L., Schiffer, M., Maróti, P., Sebban, P., and Hanson, D. K. (1997) *Biochemistry 36*, 12216−26.
20. Maróti, P., Hanson, D. K., Baciou, L., Schiffer, M., and Sebban, P. (1994) *Proc. Natl. Acad. Sci. U.S.A. 91*, 5617−21.
21. Paddock, M. L., Senft, M. E., Graige, M. S., Rongey, S. H., Turanchik, T., Feher, G., and Okamura, M. Y. (1998) *Photosynth. Res. 55*, 281−291.
22. Beroza, P., Fredkin, D. R., Okamura, M. Y., and Feher, G. (1992) in *The Photosynthetic Bacterial Reaction Center II* (Breton, J., and Vermeglio, A., Eds.) pp 363−374, Plenum Press, New York.
23. Ermler, U., Fritzsch, G., Buchanan, S. K., and Michel, H. (1994) *Structure 2*, 925−936.
24. Abresch, E. C., Paddock, M. L., Stowell, M. H. B., McPhillips, T. M., Axelrod, S. M., Soltis, S. M., Rees, D. C., Okamura, M. Y., and Feher, G. (1998) *Photosynth. Res. 55*, 119−125.
25. Stowell, M. H., McPhillips, T. M., Rees, D. C., Soltis, S. M., Abresch, E., and Feher, G. (1997) *Science 276*, 812−6.
26. Beroza, P., Fredkin, D. R., Okamura, M. Y., and Feher, G. (1995) *Biophys. J. 68*, 2233−50.
27. Lancaster, C. R., and Michel, H. (1997) *Structure 5*, 1339−59.
28. Knapp, E. W., Schulten, K., and Schulten, Z. (1980) *Chem. Phys. 46*, 215−229.
29. Pomes, R., and Roux, B. (1996) *Biophys. J. 71*, 19−39.
30. Pomes, R., and Roux, B. (1996) *Biophys. J. 71*, 33−40.
31. Cao, Y., Varo, G., Chang, M., Ni, B., Needleman, R., and Lanyi, J. K. (1991) *Biochemistry 30*, 10972−10979.
32. Luecke, H., Richter, H. T., and Lanyi, J. K. (1998) *Science 280*, 1934−1937.
33. Martinez, S. E., Cramer, W. A., and Smith, J. L. (1995) *Biophys. J. 68*, A246.
34. Ostermeier, C., Harrenga, A., Ermler, U., and Michel, H. (1997) *Proc. Natl. Acad. Sci. U.S.A. 94*, 10547−53.
35. Riistama, S., Hummer, G., Puustinen, A., Dyer, B. R., Woodruff, W. H. and Wikström, M. (1997) *FEBS Lett. 414*, 275−280.
36. Rottenberg, H. (1998) *Biochim. Biophys. Acta. 1364*, 1−16.
37. Baciou, L., and Michel, H. (1995) *Biochemistry 34*, 7967−72.
38. Baciou, L., and Michel, H. (1995) in *Photosynthesis: from light to biosphere* (Mathis, P., Ed.) pp 683−686, Kluwer Academic Publishers, Dordrecht, The Netherlands.
39. Farchaus, I. W., and Oesterhelt, D. (1989) *EMBO J. 8*, 47−54.
40. Kunkel, T. A. (1985) *Proc. Natl. Acad. Sci. U.S.A. 82*, 488−492.
41. Williams, J. C., Steiner, L. A., and Feher, G. (1986) *Proteins 1*, 312−325.
42. Simon, R., Preifer, U., and Prühler, A. (1983) *Biotechnology 1*, 784−791.
43. Davis, J., Donohue, T. J., and Kaplan, S. (1988) *J. Bacteriol. 170*, 320−329.
44. Maniatis, T., Fritsch, E. F., and Sambrook, J. (1982) *Molecular Cloning. A Laboratory Manual.*, Cold Spring Harbor Laboratory Press, Cold Spring Harbor, N. Y., U.S.A.
45. Baciou, L., Bylina, E. J., and Sebban, P. (1993) *Biophys. J. 65*, 652−60.
46. Mancino, L. J., Dean, D. P., and Blankenship, R. E. (1984) *Biochim. Biophys. Acta. 764*, 46−54.
47. Kleinfeld, D., Okamura, M. Y., and Feher, G. (1984) *Biochim. Biophys. Acta. 766*, 126−140.
48. Eyring, H., Walter, J., and Kimball, G. E. (1944) *Quantum Chemistry*, Wiley, New York.
49. Baciou, L., Rivas, E., and Sebban, P. (1990) *Biochemistry 29*, 2966−76.
50. Shopes, R. J., and Wraight, C. A. (1987) *Biochim. Biophys. Acta. 893*, 409−25.
51. Sebban, P., and Wraight, C. A. (1989) *Biochim. Biophys. Acta. 974*, 54−65.
52. Gunner, M. R., and Honig, B. (1992) in *The Photosynthetic Bacterial Reaction center: Structure, Spectroscopy and Dynamics II* (Breton, J., and Vermeglio, A., Eds.) pp 403−410, Plenum Press, New York.
53. Lancaster, C. R., Michel, H., Honig, B., and Gunner, M. R. (1996) *Biophys. J. 70*, 2469−92.
54. Takahashi, E., and Wraight, C. A. (1996) *Proc. Natl. Acad. Sci. U.S.A. 93*, 2640−5.
55. Maroti, P., and Wraight, C. A. (1997) *Biophys. J. 73*, 367−81.
56. Shinkarev, V. P., Drachev, L. A., Mamedov, M. D., Mulkidjanian, A. J., Semenov, A. Y., and Verkhovsky, M. I. (1993) *Biochim. Biophys. Acta. 1144*, 285−294.
57. Pomes, R., and Roux, B. (1998) *Biophys. J. 75*, 33−40.
58. Alexov, E. G. and Gunner, M. R. (1999) *Biochemistry*, in press.
59. Roussel, A., and Cambillau, C. (1991) in *Silicon Graphics Geometry Partner Directory*, Silicon Graphics, Mountain View, CA.

BI990192E